IOPscience iopscience.iop.org

Home Search Collections Journals About Contact us My IOPscience

Tunable multimodal adhesion of three-dimensional, nanocrystalline $CoFe_2O_4$ pollen replicas

This content has been downloaded from IOPscience. Please scroll down to see the full text.

Download details:

IP Address: 130.207.78.136

This content was downloaded on 31/08/2017 at 21:01

Manuscript version: Accepted Manuscript

Goodwin et al

To cite this article before publication: Goodwin et al, 2017, Bioinspir. Biomim., at press: https://doi.org/10.1088/1748-3190/aa7c89

This Accepted Manuscript is: © 2017 IOP Publishing Ltd

During the embargo period (the 12 month period from the publication of the Version of Record of this article), the Accepted Manuscript is fully protected by copyright and cannot be reused or reposted elsewhere.

As the Version of Record of this article is going to be / has been published on a subscription basis, this Accepted Manuscript is available for reuse under a CC BY-NC-ND 3.0 licence after the 12 month embargo period.

After the embargo period, everyone is permitted to copy and redistribute this article for non-commercial purposes only, provided that they adhere to all the terms of the licence https://creativecommons.org/licences/by-nc-nd/3.0

Although reasonable endeavours have been taken to obtain all necessary permissions from third parties to include their copyrighted content within this article, their full citation and copyright line may not be present in this Accepted Manuscript version. Before using any content from this article, please refer to the Version of Record on IOPscience once published for full citation and copyright details, as permission will likely be required. All third party content is fully copyright protected, unless specifically stated otherwise in the figure caption in the Version of Record.

When available, you can view the Version of Record for this article at: http://iopscience.iop.org/article/10.1088/1748-3190/aa7c89

Tunable Multimodal Adhesion of Three-Dimensional, Nanocrystalline $CoFe_2O_4$ Pollen Replicas

W. Brandon Goodwin,[a,‡] Donglee Shin,[b,‡] Daniel Sabo,[c] Sunghwan Hwang,[d] Z. John Zhang,[c] J. Carson Meredith,[*,b] and Kenneth H. Sandhage[*,a,d]

Three-dimensional (3-D) replicas of sunflower pollen microparticles, comprised of a multicomponent magnetic spinel ferrite ($CoFe_2O_4$) with tailorable adhesive properties, have been synthesized for the first time via a conformal layer-by-layer (LbL) surface sol-gel (SSG) deposition process followed by organic pyrolysis and oxide compound formation at a peak temperature of 600°C to 900°C. These high-fidelity ferrite pollen replicas exhibited multimodal (van der Waals, vdW, and magnetic) adhesion that could be tuned via control of the $CoFe_2O_4$ nanoparticle and crystal sizes. The $CoFe_2O_4$ pollen replicas exhibited a non-monotonic change in short-range (~ 10 nm) vdW adhesion with an increase in the peak firing temperature, which was consistent with the counteracting effects of particle coarsening on the size and number of nanoparticles present on the sharp tips of the echini (spines) on the pollen replica surfaces. The longer-range (up to ~1 mm) magnetic force of adhesion increased monotonically with an increase in firing temperature, which was consistent with the observed increases in the values of the saturation and remanent magnetization of $CoFe_2O_4$ with an increase in average nanocrystal size. By adjusting the nanocrystal/nanoparticle sizes of the $CoFe_2O_4$ pollen replicas, the total force of adhesion (vdW + magnetic) to a magnetic substrate could be increased by a factor of ~3 relative to native pollen grains.

[a] *School of Materials Science and Engineering, Georgia Institute of Technology, Atlanta, GA 30332, United States*
[b] *School of Chemical and Biomolecular Engineering, Georgia Institute of Technology, Atlanta GA 30332, United States*
[c] *School of Chemistry and Biochemistry, Georgia Institute of Technology, Atlanta GA 30332, United States*
[d] *now at School of Materials Engineering, Purdue University, W. Lafayette, IN 47907, United States*
* Corresponding Authors: E-mail: sandhage@purdue.edu (K.H.S.), carson.meredith@chbe.gatech.edu (J.C.M.)
‡ These authors contributed equally.

Electronic Supplementary Information (ESI) available: Values of the XRD-determined average crystal radii and the FEG-SEM-determined average nanoparticle radii on the spine tips of $CoFe_2O_4$ pollen particle replicas fired at peak temperatures of 600°C to 900°C (Table S1); plots of the pseudo-Voigt profile fits and Caglioti fits, and Williamson-Hall plots for $CoFe_2O_4$ pollen particle replicas fired at peak temperatures of 600°C to 900°C (Figures S1-S3). See DOI: 10.1039/x0xx00000x

Introduction

The adhesive behavior of inorganic microparticles is of appreciable importance for a variety of established and nascent materials and technologies, including paints, inks, xerography, tagging/labeling, semiconductor device processing, water purification, (bio)chemical separations, particulate removal from exhaust streams, targeted drug delivery, catalysis, composite processing, anti-fouling coatings, and assembly of hierarchical structures.[1] Nonetheless, the ability to tailor the adhesion of microscale particles by selecting and controlling the 3-D shapes, surface features, and inorganic chemistries of such particles remains a non-trivial challenge.

One approach for generating microscale particles of complex, but controlled shape and of tailorable synthetic inorganic chemistry is to convert readily-available 3-D microparticle templates of a given naturally-occurring composition into a desired inorganic material via a shape-preserving coating[2] and/or reaction[3] process (that is, to preselect a template of desired shape and then alter the template chemistry while preserving the template shape). Among the most abundant of naturally-occurring (low-cost, sustainable) adhesive microparticle templates with a wide range of selectable 3-D shapes are pollen particles.[4] Several authors have chemically-modified pollen to endow such particles with desired absorptive, photocatalytic, and electrochemical properties.[5] Prior work has shown that the hydroxyl-rich nature of the exine of pollen particles, as well as of other biological surfaces, allows for direct and conformal oxide coating via the layer-by-layer (LbL) surface sol-gel (SSG) process.[6] However, the LbL coating and conversion of pollen particles into 3-D replicas comprised of a multicomponent (complex) oxide that can be tailored for enhanced adhesion has not been reported. The purpose of the present paper is to demonstrate, for the first time, that the LbL SSG process may be used to convert pollen particles into high-fidelity 3-D replicas comprised of a phase-pure binary ferrite ($CoFe_2O_4$) magnetic compound with a nanostructure that can be adjusted so as to tailor both short-range (van der Waals, vdW) and long-range (magnetic) adhesion forces.

Accepted Manuscript

Experimental

Pollen Preparation. The conversion of sunflower (*Helianthus annuus*) pollen (Greer Laboratories, Lenoir, NC USA) into replicas comprised of cobalt ferrite, $CoFe_2O_4$, has been examined in this work. The pollen grains were first cleaned by immersion in a mixture of chloroform and methanol (3:1)[7] for 24 h, followed by deposition onto filter paper (P5, Fisher Scientific, Pittsburgh, PA USA) and drying under vacuum at 60°C for 12 h. A second immersion was conducted in 1 M hydrochloric acid (VWR, Suwanee, GA USA) for 1 h to remove residual inorganic material, followed by rinsing 3 times with de-ionized water, and drying by vacuum aspiration at room temperature for 5 min.

Computer-automated LbL SSG Deposition. Fe-O-bearing and Co-O bearing coatings were sequentially applied to cleaned, acid-washed pollen grains via a computer-controlled LbL SSG deposition system[8] located within a N_2-atmosphere glovebox. Pollen grains were first immersed for 10 min with stirring in a solution of 0.0125 M Fe(III) isopropoxide or 0.0125 M Co(II) isopropoxide (both from Alfa Aesar, Ward Hill, MA USA) in anhydrous 2-propanol ($\geq$99.8% purity, Acros Organics, Geel, Belgium) to allow for the chemisorption of a Fe-O-bearing or Co-O-bearing layer, respectively. After rinsing three times with anhydrous 2-propanol and vacuum filtration, the pollen grains were immersed in de-ionized water (DIW) with stirring for 5 min, to allow for hydrolysis of the chemisorbed alkoxide layer. The pollen grains were then rinsed three times with the anhydrous 2-propanol, filtered under vacuum, and dried by vacuum aspiration for 5 min. This process (alkoxide exposure, alcohol rinsing, water exposure, alcohol rinsing, drying) was repeated 50 times (for a total of 51 cycles) to build up a continuous and conformal coating. The pollen particles were coated using alternating Fe-O and Co-O deposition cycles, in a Fe-O:Co-O cycle ratio of 2:1, so as to achieve the desired stoichiometry for the $CoFe_2O_4$ spinel compound (i.e., a total of 17 Co-O cycles and 34 Fe-O cycles were used).

Thermal Processing and Thermal Analysis. The coated pollen particles were heated in air at a rate of 3°C min^{-1} to a peak temperature of 600°C, 700°C, 800°C, or 900°C and held at this peak temperature for 2 h to allow for organic pyrolysis and $CoFe_2O_4$ formation. The specimens were then cooled in air at a rate of 2°C min^{-1} to room temperature. Thermogravimetric (TG) analyses (Model STA 449C, Netzsch, Wolverhampton, UK) were conducted on uncoated or coated pollen grains in a flowing (50 cm^{3}min^{-1}) synthetic air mixture using a heating rate of 5°C min^{-1} up to 600°C and then holding at 600°C for 6 h.

Substrate Preparation and Characterization. The adhesion of pollen replica microparticles was tested using four types of substrates: gold (Au), copper (Cu), nickel (Ni), and a nickel-coated neodymium-iron-boron alloy (referred to herein simply as the Ni-Nd substrate), with the latter substrate used to evaluate magnetic adhesion. The gold and copper substrates consisted of 100 nm thick films on polished (0.3 ± 0.1 nm RMS roughness) silicon substrates (100 mm diameter, 100 prime grade, Silicon, Inc., Boise, ID USA). Au and Cu deposition were conducted by electron beam evaporation (CHA Mark-40 system, CHA Industries, Fremont, CA USA) at a rate of 2Å/sec with a background pressure of 10^{-6} torr. Nickel foil substrates (grade 200, 99.5% purity, 0.15 mm thick, Shop-Aid, Inc., Woburn, MA USA) with an area of 38.5 mm^2 were prepared by electropolishing in a 8.9 mol L^{-1} sulfuric acid solution using a platinum rod cathode with a constant 1.3 A current for 120 sec. The Ni-Nd substrate consisted of an axially-poled, Nd-Fe-B-based alloy permanent magnet (Model ND022N-35, 5 mm diameter disk, 1.5 mm thick, Master Magnetics, Inc., Castle Rock, CO USA) onto which was attached the polished Ni foil.[6f,6g] Prior to use in adhesion measurements, the substrates were ultrasonically cleaned (Model FS20 ultrasonic bath, Fisher Scientific, Pittsburgh, PA USA) in acetone (99.5% purity, BDH Chemical Ltd., Radnor, PA USA) for 10 min at room temperature. The surface roughness of each type of substrate was evaluated with a scanning probe microscope (Dimension 3100 SPM equipped with a Nanoscope V Controller, Veeco Instruments, Inc., Plainview, NY USA) operated in tapping mode at 200-400 kHz using a pyramidal tip silicon cantilever (Applied NanoStructures, Inc., Santa Clara, CA USA). For each particular substrate, 3 randomly-located scans (10 µm x 10 µm) were conducted, and 4 smaller regions (1 µm x 1 µm) from within each scan were randomly selected. The average roughness value for a given substrate was obtained using the data from these 12 regions.

Pollen Replica Characterization. Scanning electron microscopy was conducted with a field emission gun instrument (1530 FEG SEM, Carl Zeiss SMT, Ltd., Thornwood, NY USA). FEG-SEM images of the end tips of the spines (echini) of $CoFe_2O_4$ pollen replicas were used to evaluate the sizes of oxide nanoparticles present at such spine tips. For each type of $CoFe_2O_4$ pollen replica examined (i.e., for replicas fired at a peak temperature of 700°C, 800°C, or 900°C), the sizes of 20 oxide nanoparticles on each of 3 spine tips (for a total of 60 measurements per type of replica) were evaluated to obtain an average oxide nanoparticle diameter. For the $CoFe_2O_4$ pollen replica examined fired at a peak temperature of 600°C, the individual nanoparticles located at the spine tips were too fine to allow for unambiguous nanoparticle diameter measurement by the FEG-SEM. The FEG-SEM was equipped with an energy dispersive X-ray spectrometer (EDS, INCA Model 7426, Oxford Instruments, Abingdon, Oxfordshire UK) for local semi-quantitative elemental analyses of individual pollen replicas. Quantitative elemental analyses of 1 g batches of $CoFe_2O_4$ replica particles were obtained (Laboratory for

Accepted Manuscript

Environmental Analyses, University of Georgia, Athens, GA USA) by inductively-coupled plasma mass-spectroscopy (ICP-MS, PerkinElmer Model Elan 9000, Waltham, MA USA). For ICP-MS analyses, the $CoFe_2O_4$ replica particles were dissolved in an aqua regia solution heated within a sealed Teflon container in a microwave system (MDS 81D system, CEM Corp., Matthews, NC USA) operated at 400 W for 25 min. ICP-MS analyses were conducted on three different sample batches to obtain an average Fe/Co ratio. For phase identification and evaluation of average crystal size by X-ray diffraction (XRD) analyses, pollen replica microparticles were dispersed in isopropyl alcohol (IPA), and the microparticle/IPA slurry was then deposited via pipette onto a low background substrate (i.e., a quartz crystal cut at an angle of 6^o from the (0001) plane, The GEM Dugout, State College, PA, USA). After allowing the IPA to dry, XRD analyses were conducted at room temperature using Cu-Kα1 radiation emanating from a 1.8 kW X-ray tube with a copper anode (45 kV, 40 mA) equipped with an incident beam Johansson monochromat0r (X'Pert Pro Alpha-1, PANalytical B.V., Almelo, Netherlands). The incident beam optics were outfitted with 0.04 rad soller slits, a 2^o fixed anti-scatter slit, a programmable divergence slit set to a 5.5 mm irradiated length, and a 10 mm mask. The diffracted beam optics were outfitted with a 5.5 mm anti-scatter slit and 0.04 rad soller slits placed before the X'Celerator linear detector (PANalytical B.V.). Each XRD pattern was produced with a summation of 40 similar scans of 30 min duration, with each conducted using the Bragg-Brentano geometry over a 2θ range of 20^o to 90^0 with a step size of 0.017^o 2θ. The minimum Pulse Height Discrimination setting for the X'Celerator detector was increased from 36 to 42 to enhance detection of the diffracted signal relative to fluorescence photons from the Fe and Co atoms.[9] Phase identification and average crystallite radius (R_C) values were determined with HighScore Plus software (PANalaytical B.V.) using a Pseudo-Voigt profile fit function.[10] A silicon line standard (Standard Reference Material 640c, National Institute of Standards and Technology/NIST, Gaithersburg, MD) was used to determine the instrument-associated broadening of diffraction peaks. Williamson-Hall plots were used to determine values of the average $CoFe_2O_4$ crystal size for pollen replicas fired at different peak temperatures. Lattice fringe imaging of $CoFe_2O_4$ nanocrystals was conducted via high-resolution transmission electron microscopy (Titan 80-300 kV Environmental TEM, FEI, Hillsboro, OR, USA) of electron transparent cross-sections prepared by focused ion beam milling (Nova 200 Nanolab DualBeam, FEI).

Adhesion Measurements. Adhesion measurements were conducted using a single particle (a native cleaned sunflower pollen particle or a $CoFe_2O_4$ replica particle) attached to an atomic force microscope (AFM) cantilever. A given particle was attached to a tipless silicon AFM cantilever (FORT-TL, Applied NanoStructures, Inc.) using a small amount of epoxy resin (Epoxy Marine, Loctite, Westlake, OH USA). For each type of pollen-shaped particle (cleaned sunflower pollen, or $CoFe_2O_4$ pollen replica) and firing condition used (no firing or firing a peak temperature of 600°C, 700°C, 800°C, or 900°C), 3 single-particle-bearing cantilever probes were prepared (for a total of 15 particle/cantilever probes). The spring constants, as determined with the scanning probe microscope, of the sunflower-pollen-bearing cantilever probes and the $CoFe_2O_4$ replica-bearing cantilever probes fired at peak temperatures of 600°C, 700°C, 800°C, or 900°C fell in the ranges of 1.834-2.336 N/m, 0.867-0.973 N/m, 0.899-1.145 N/m, 1.040-1.208 N/m, and 1.020-1.287 N/m, respectively. The adhesion force between an individual sunflower pollen particle, or $CoFe_2O_4$ replica particle, and a particular substrate was evaluated with the scanning probe microscope operated in contact mode. For each particular particle/cantilever probe and particular substrate, 10 separate force-distance scans were obtained, and the depth of adhesion wells upon retraction were averaged. The load force applied during the contact adhesion measurements was 2.5 nN. The ambient relative humidity in the laboratory during the adhesion measurements ranged from 30 to 35%. The magnetic hysteresis behavior of the $CoFe_2O_4$ replica particles was evaluated at 5K and at 300 K using a superconducting quantum interference device (SQUID) magnetometer (Model MPMS-5S, Quantum Design, San Diego, CA USA) with an applied magnetic field up to 5 T.

Results and Discussion

A computer-automated LbL SSG deposition process was used to apply thin, conformal Co-O-bearing and Fe-O-bearing layers to sunflower pollen particles. Representative secondary electron (SE) images of a cleaned native (uncoated) sunflower pollen particle, and a sunflower pollen particle that had been exposed to 51 SSG deposition cycles (17 Co-O cycles and 34 Fe-O cycles for a Co-O:Fe-O cycle ratio of 1:2), are shown in Figures 1a and 1b, respectively. The roughly spherical shape and sharp echini (spines) of the native sunflower pollen particles were well preserved in the Co-Fe-O-coated particles. The apparent absence of cracks or gaps in the coated particle surface was also consistent with the highly-uniform chemisorption of Co(II) isopropoxide and Fe(III) isopropoxide on the pollen exine (outer layer) during the SSG coating process. Such continuous and conformal Co-Fe-O deposition indicated that a high and uniform density of surface hydroxyl reaction sites was available on the pollen

Accepted Manuscript

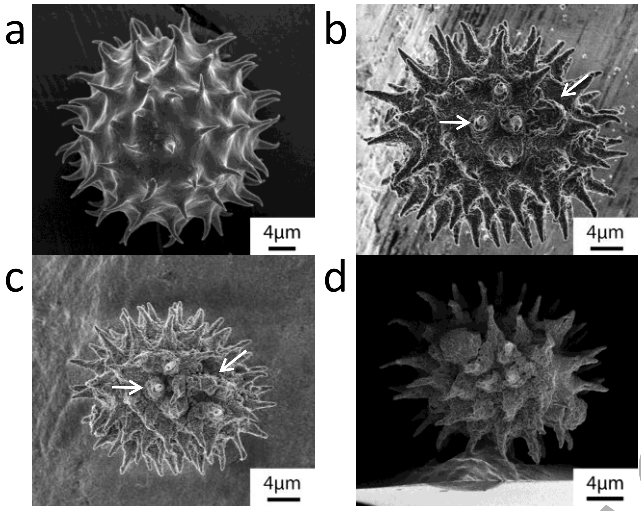

Figure 1. SE images of sunflower pollen particles at various stages of conversion into $CoFe_2O_4$: (a) a cleaned, uncoated sunflower grain; (b) a Co-Fe-O-coated pollen grain after exposure to 51 SSG deposition cycles (with 17 cycles involving a Co(II) isopropoxide solution and 34 cycles involving a Fe(III) isopropoxide solution) and (c) the $CoFe_2O_4$ replica of the Co-Fe-O-coated pollen grain shown in (b) generated by thermal treatment at a peak temperature of 800°C for 2 h in air (white arrows in (b) and (c) reveal some of the particular features preserved after thermal treatment); (d) a cantilever probe bearing a single $CoFe_2O_4$ sunflower pollen grain replica generated by thermal treatment at a peak temperature of 900°C for 2 h in air.

surface for reaction with these cobalt and iron alkoxides (note: the exine of pollen is comprised of sporopollenin, which is a complex polymer consisting of carboxylic acids cross-linked with aliphatic chains[11]). A SE image obtained after firing the Co-Fe-O-coated pollen particle shown in Figure 1b (at a peak temperature of 800°C for 2 h in air) is shown in Figure 1c. While this thermal treatment resulted in pollen particle shrinkage, the 3-D shape and surface features of the coated particle were well preserved in the fired replica. The white arrows shown in Figures 1b and 1c identify some of the specific features that were preserved in this same particle before and after firing. Such 3-D shape preservation was also observed for Co-Fe-O-coated particles exposed to peak temperatures of 600°C to 900°C for 2 h in air. TG analyses of uncoated and Co-Fe-O-coated sunflower pollen confirmed that organic pyrolysis was completed well before 2 h at 600°C (Figure 2). ICP-MS analyses of three 1 g batches of these fired pollen replicas yielded an average Fe:Co atomic ratio of 1.91$\pm$0.05, which was within the composition range reported by Takahashi and Fine[12] for a single $(Co,Fe)_3O_4$ spinel phase at equilibrium with air at 500-900°C. Local SEM/EDS analyses of individual fired pollen replicas yielded similar Fe:Co atomic ratios.

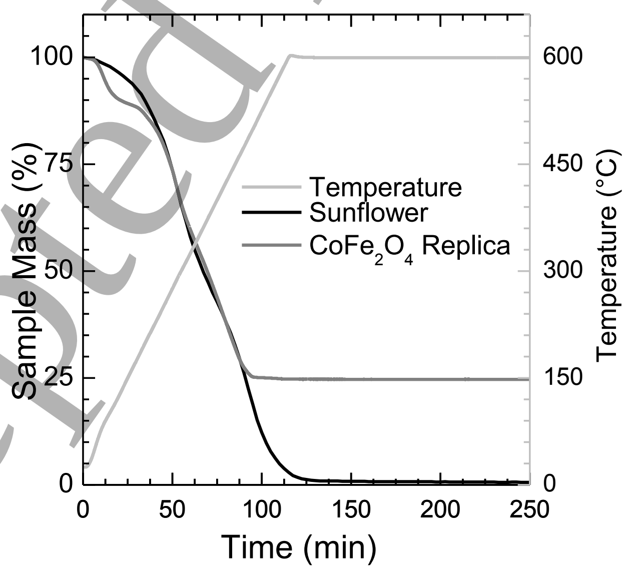

Figure 2. Thermogravimetric (TG) analysis of cleaned (uncoated) sunflower pollen grains and Co-Fe-O-coated sunflower pollen grains (51 SSG deposition cycles) during heating in flowing (50 $cm^3\ min^{-1}$) synthetic air at 5°C min^{-1} to 600°C and then holding at this temperature.

X-ray diffraction (XRD) analyses were conducted to determine the crystalline phase content and average crystal size of the oxide-converted pollen replicas. XRD patterns obtained from the Co-Fe-O-coated pollen grains

Accepted Manuscript

that had been thermally treated in air for 2 h at peak temperatures of 600-900°C are shown in Figure 3. All of the observed diffraction peaks for each firing condition could be attributed to the $CoFe_2O_4$ compound[13], which was consistent with the formation of a single spinel phase after each thermal treatment. A higher magnification view of the highest intensity (311) diffraction peaks provided in Figure 3b indicated that the values of the diffraction peak width at half maximum intensity narrowed as the peak firing temperature increased from 600°C to 900°C for the same hold time, which was consistent with an increase in the average crystal size with increasing temperature. Full pattern profile fitting, utilizing the following Pseudo-Voigt profile fit function[10], was conducted

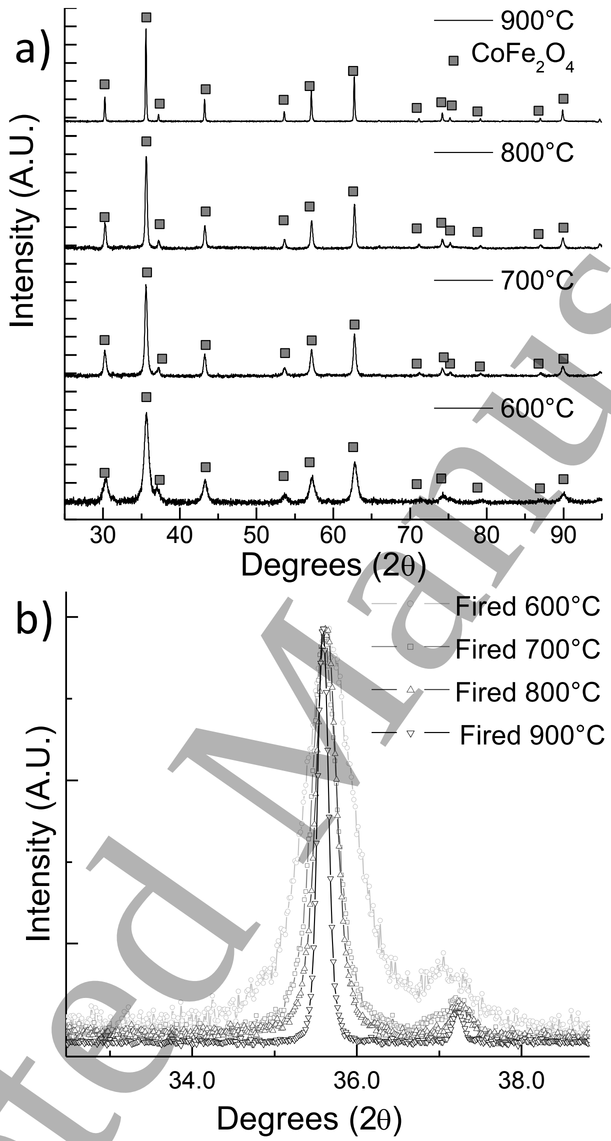

Figure 3. (a) XRD patterns obtained from Co-Fe-O-coated pollen grains after thermal treatment in air at a peak temper-ature of 600°C, 700°C, 800°C, or 900°C for 2 h. b) a magnified view of (311) diffraction peaks for these $CoFe_2O_4$ specimens revealing a monotonic decrease in peak widths at half maximum intensity with an increase in the peak firing temperature.

on each of these XRD patterns (Figure S1 in Supplementary Information) to obtain values of the full diffraction peak width at half maximum intensity, H_k, for each diffraction peak.

$$G_{ij} = \gamma \frac{C_0^{1/2}}{H_k \pi}\left[1 + C_0 1 X_{ij}^2\right]^{-1} + (1-\gamma)\frac{C_1^{1/2}}{H_k \pi^{1/2}} exp\left[-C_1 X_{ij}^2\right] \qquad (1)$$

In equation (1): $C_0 = 4$; $C_1 = 4\ln 2$; X_{ij} is related to the peak position, 2θ, and H_k by equation (2) below; and γ is a refinable mixing parameter of Gaussian and Lorentzian peak shapes given by equation (3) below.

$$X_{ij} = \left(2\theta_j 2\theta_k\right)/H_k \qquad (2)$$

$$\gamma = \gamma_1 + \gamma_2 2\theta + \gamma_3 (2\theta)^2 \qquad (3)$$

Accepted Manuscript

The H_k values were then fitted to the following Caglioti equation (with U, V, and W as fitting parameters, Figure S2 in Supplementary Information).[14]

$$H_k = (Utan^2\theta + Vtan\theta + W)^{1/2} \quad (4)$$

The Caglioti-fitted equations for H_k were used to calculate the structural peak breadth, B_{Str}, using the following equation:

$$B_{Str} = B_{Obs} - B_{Instr} \quad (5)$$

where B_{Obs} refers to the experimental measurement of the diffraction peak width at half maximum intensity and B_{Instr} refers to the instrument-associated broadening of the diffraction peak at half maximum intensity (with the latter value determined from diffraction measurements obtained using the NIST silicon line standard). B_{Obs} and B_{Instr} are constructed by combining both net Gaussian and Lorentzian broadenings components as seen below:

$$B = B_G/\left(-0.4K\sqrt{\pi} + 0.5C - 0.234Ke^{-2.176K}\right) \quad (6)$$

with $$K = B_L/\left(\sqrt{\pi}B_G\right) \quad (7)$$

and $$C = \sqrt{\pi K^2 + 4} \quad (8)$$

The values of B_{Str} were then fitted to the Williamson-Hall plot using the following equation[15] (Figure S3 in Supplementary Information):

$$B_{Str}cos\theta = \frac{2\lambda}{R} + 4\varepsilon sin\theta \quad (9)$$

where λ is the X-ray wavelength, R is the average crystal radius, and ε is the microstrain. The resulting values of the average $CoFe_2O_4$ crystal radii increased monotonically with an increase in the peak firing temperature (Figure 4), and ranged from 5$\pm$2 nm after thermal treatment at a peak temperature of 600°C to 38$\pm$6 nm after treatment at a peak temperature of 900°C (see also Table S1 in Supplemental Information). An electron-transparent cross-section of the $CoFe_2O_4$ specimen prepared with a peak firing temperature of 700°C was also examined via transmission electron microscopy. High-resolution lattice fringe images of this specimen (Figure S4 in Supplementary Information) revealed nanocrystals with radii of 10$\pm$3 nm, which was consistent with the data in Figure 4.

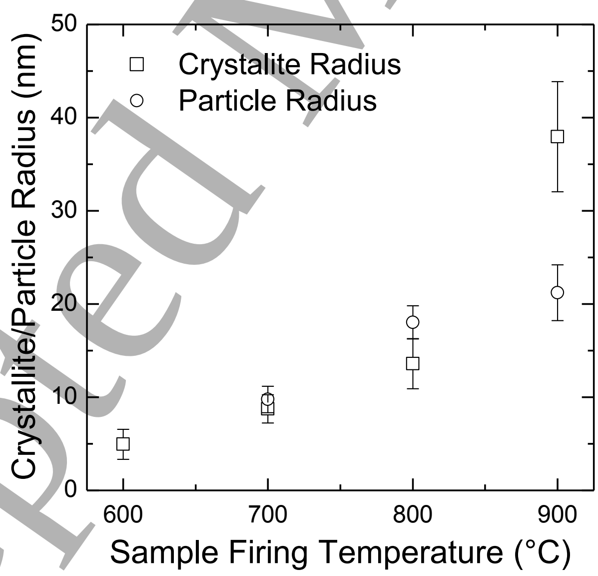

Figure 4. Values of the average crystallite and nanoparticle radii of $CoFe_2O_4$ pollen replicas (determined from XRD and FEG-SEM analyses, respectively) plotted as a function of the peak firing temperature. The error bars indicate a range of $\pm$ 1 standard deviation of the measurement.

Higher magnification SE images were obtained of the individual echini (spine) tips of the $CoFe_2O_4$ pollen replicas (Figure 5) to allow for evaluation of the sizes of oxide nanoparticles present on the echini surfaces. The average values of the $CoFe_2O_4$ nanoparticle radii obtained at the spine tips from such FEG-SEM analyses are plotted in Figure 4. As for the case with the XRD-derived average crystal radii values, the values of the FEG-SEM-

Accepted Manuscript

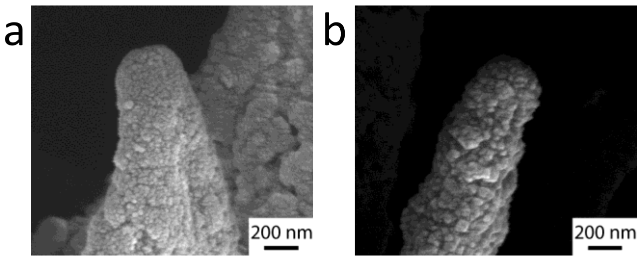

Figure 5. SE images of the tips of preserved echini of $CoFe_2O_4$ pollen replicas fired in air for 2 h at a peak temperature of: a) 700°C and b) 900°C.

derived average nanoparticle radii for the $CoFe_2O_4$ replicas increased with an increase in the peak firing temperature.

Contact mode AFM measurements were conducted to evaluate the short-range (van der Waals, vdW) force of adhesion of $CoFe_2O_4$ sunflower pollen replica particles (attached to AFM cantilevers) to three different planar metallic (non-magnetic) substrates of similar surface roughness: Au, Cu, and Ni substrates. (Note: the values of average surface roughness of the Au, Cu, and Ni substrates were 1.1±0.2 nm, 0.9±0.2 nm, and 0.9±0.2 nm, respectively.) Plots of the measured average vdW adhesion force of the $CoFe_2O_4$ pollen replicas on each substrate, as a function of the average size of surface nanoparticles (obtained from SEM analyses of the echini replica tips of the 700-900°C samples) and as a function of the average crystallite size (obtained from XRD analyses for the 600-900°C samples as discussed above), are presented in Figures 6a and 6b, respectively. Figures 6a and 6b reveal similar non-monotonic trends for all three metallic substrates; that is, the average adhesion force initially decreased with increasing crystal and nanoparticle size, reached minimum values at average crystal and nanoparticle radii of 14±3 nm and 18±2 nm, respectively (at a peak firing temperature of 800°C), and then increased with further increases in average crystal and nanoparticle radii. While prior work has indicated that the short-range vdW adhesion of nanocrystalline iron oxide replicas (Fe_2O_3, Fe_3O_4) of sunflower pollen particles to metallic substrates was consistent with the contact of one or two nanocrystals on the echini tips with the substrates, the influence of variations in crystal/nanoparticle size on vdW adhesion was not previously explored.[6f,g]

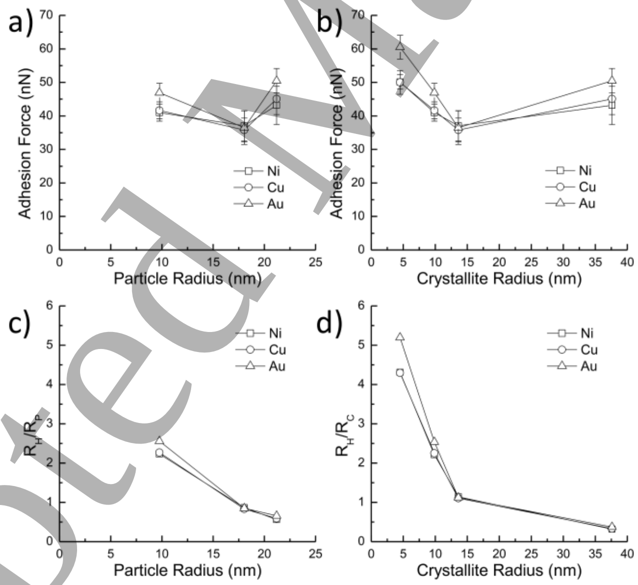

Figure 6. Average values of the short-range, vdW-based adhesion force of $CoFe_2O_4$ sunflower pollen replicas on planar metallic substrates, obtained from contact mode AFM measurements, plotted as a function of: a) the average surface nanoparticle radii on the echini tips (from FEG-SEM analyses) and b) the average crystallite radii (obtained from XRD analyses). The error bars indicate 95% confidence intervals. (c) The ratio of the effective contact radius obtained with the use of the Hamaker model to the average surface nanoparticle radius obtained by SEM measurements, (R_H/R_P) plotted versus R_P. (d) The ratio of the effective contact radius obtained with the use of the Hamaker model to the average crystallite radius obtained by XRD analyses, (R_H/R_C), plotted versus R_C.

The non-monotonic variations in the vdW adhesion force with increases in the average values of crystal and nanoparticle sizes of the $CoFe_2O_4$ pollen replicas have been evaluated in the present case with the use of the following simple Hamaker model for the adhesion force between a sphere and a plate[16]:

$$F_{vdw} = -\frac{A_{132}}{24R}\left(\frac{2}{x} - \frac{1}{x^2} - \frac{2}{x+1} - \frac{1}{(x+1)^2}\right) \qquad (10)$$

Accepted Manuscript

where A_{132} is the nonretarded Hamaker constant of material 1 (the metal substrate) interacting with medium 2 ($CoFe_2O_4$) across a medium 3 (air); R is the contact radius of the sphere (in the present case, a spherical nanoparticle or crystal); $x = D/2R$; and D is the separation distance between the sphere and the plate. An approximate value of A_{132} (≈ 3.3 X 10^{-19} J) for $CoFe_2O_4$ sunflower pollen particle replicas on the metal substrates was calculated by using the following equation[17]:

$$A_{132} \approx \left(\sqrt{A_{11}} - \sqrt{A_{33}}\right)\left(\sqrt{A_{22}} - \sqrt{A_{33}}\right) \qquad (11)$$

with the values of A_{11} (≈ 4 X 10^{-19} J)[17] and A_{22} (≈ 4 X 10^{-19} J)[18] obtained from the literature, and with $A_{33} = 0$. The value of F_{vdw} predicted by equation (10) should be linearly proportional to R for cases where D is much smaller than 2R (i.e., for these cases, the second term on the right side of equation (10), $A_{132}R/6D^2$, becomes dominant). For contact radii in the range of values of the measured crystal/particle radii shown in Figures 6a and 6b, the predicted values of the vdW adhesion force associated with such a single crystal/particle contact are shown in Figure 7a. The monotonic dependence of the vdW adhesion force on crystal/nanoparticle radius predicted by such a single contact radius model was inconsistent with the non-monotonic dependence observed experimentally (Figures 6a and 6b). Equation (10) was then used to extract the value of the effective contact radius (R_H) for each sample from the average measured adhesion force value, by solving for the R value (called R_H) that resulted in a force equal to the measured value. The ratio of R_H to the measured average surface nanoparticle radius (R_P) or average crystal radius (R_C) is plotted versus R_P or R_C in Figures 6c and 6d. An R_H/R_P or R_H/R_C ratio of unity would be consistent with adhesion via the contact of a single nanoparticle or crystal according to equation (10). As seen in Figures 6c and d, this condition was roughly met at the values of R_P = 18 nm and R_C = 14 nm, (i.e., for the replicas fired at a peak temperature of 800°C). In this case, the measured adhesion force values of 35-38 nN were close to the values of 27 nN (with R_C = 14 nm) or 36 nN (with R_P = 18 nm) predicted by equation (10) for a single contact Hamaker model. However, the extracted values of R_H were noticeably different from the measured values of R_P and R_C for the samples fired at peak temperatures of 600°C and 700°C, which indicated that a single contact point could not explain the short-range adhesion of replicas fired at these temperatures.

For a curved surface (such as an echini tip) containing fine nanoparticles with similar radii of R_S, the number of particles located within the vdW interaction region with the substrate will depend on the particle size, as illustrated in Figure 7b. At a sufficiently large particle size, a single contacting particle will dominate the short-

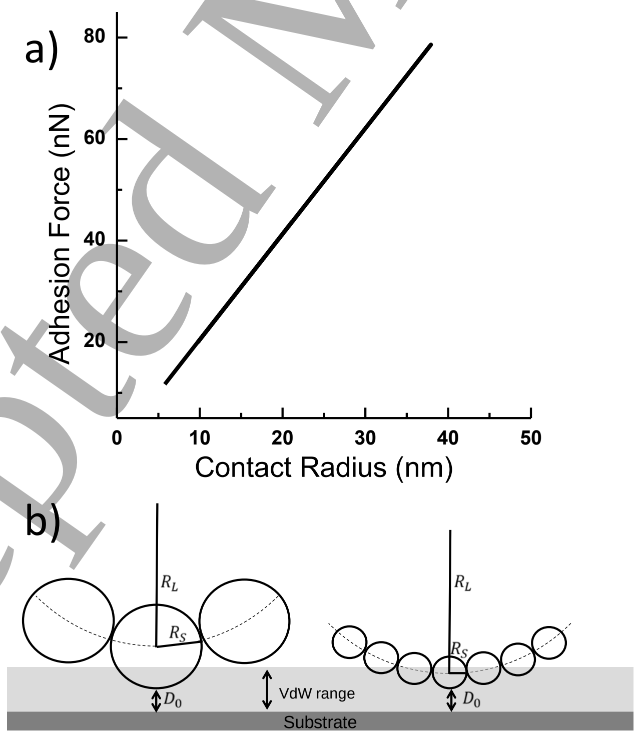

Figure 7. a) Estimated values of the short-range vdW adhesion force as a function of contact radius for a single crystal/particle contact. b) 2-D diagram illustrating a multiparticle model of vdW adhesion consisting of an assembly of symmetrical small spheres of radius R_S arranged on a larger hemisphere of radius R_L).

Accepted Manuscript

range van der Waals attraction of the curved surface to the substrate (Figure 7b, left side of the illustration).[19] As mentioned above, such a single-contact model should result in a monotonic increase in the adhesion force with a further increase in the particle radius (Figure 7a). However, for smaller R_S values, the adhesion force will be dependent on multiple particles interacting within the short vdW interaction range. In this "multiparticle" attraction case, an increase in the vdW force may be observed with a decrease in nanoparticle size, due to the corresponding increase in the number of particles on the curved surface that can interact with the adjacent flat surface (Figure 7b, right side of the illustration). The switching between these two competing effects of particle size on the total vdW adhesion is expected to occur at a particle radius of roughly the vdW interaction range (i.e., on the order of 10^1 nm), which was consistent with the experimentally-observed minima in Figures 6a and 6b.

Further support for this hypothesis was obtained with the aid of a simple computer simulation. The number of nanoparticles in the vdW interaction zone (~10 nm) of the flat substrate surface, and the positions of such nanoparticles relative to the flat substrate, were determined by modeling the polycrystalline replica echini (spine) tip as being comprised of perfectly packed small spheres located on a large hemisphere; that is, the large hemisphere represents the replica echini tip (average radius, 196 ± 17 nm) and the small spheres represent the nanoparticle/crystallites on the echini tip, as illustrated in Figure 8a for small spheres of size R_S = 8 nm and 16 nm. Using this model, the number of spheres on the echini tip in the range of 10 nm from the flat substrate is plotted over a range of representative small sphere (crystallize) sizes, R_S, in Figure 8b. This figure indicates that the number of adhesive contacts can be quite large when R_S is small (e.g., less than 5 nm), but decreases relatively

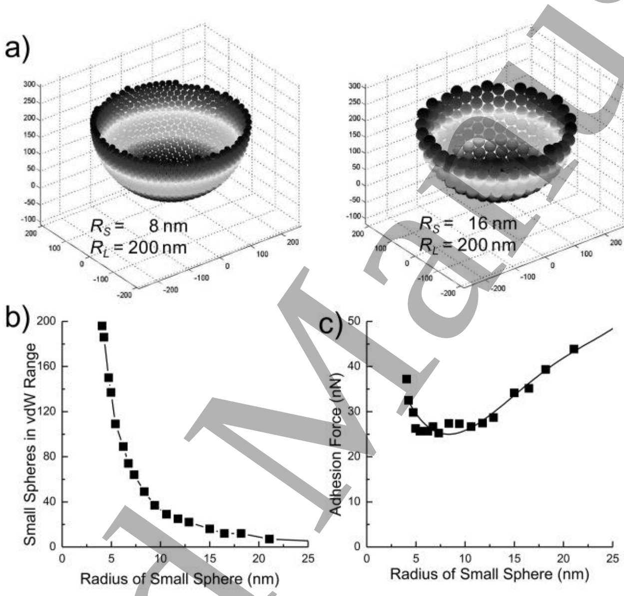

Figure 8. a) 3-D schematic models of nanoparticles on echini (spine) tips consisting of perfectly packed small spheres on a large hemisphere (with $\mathbf{R_s}$- radius of small spheres, $\mathbf{R_L}$- radius of the large hemisphere). Calculated relationships are shown between: b) the number of small spheres in the vdW range (~ 10 nm) and the radii of small spheres ($\mathbf{R_s}$), and c) the total vdW adhesion force and the radii of small spheres ($\mathbf{R_s}$).

slowly with R_S for R_S values above ~10 nm. The adhesion force to the flat substrate of each small sphere on the echini tip that is within the vdW interaction zone was calculated using equation (10) by taking the separation distances from the substrate as D = H + 0.165 nm (cutoff distance)[17] and by using the previously estimated Hamaker constant of $A_{132} \approx 3.3 \times 10^{-19}$ J. The total adhesion between the large hemisphere (echini tip composed of many small particles/crystallites) and the flat substrate was then calculated by summation of the adhesion forces of each small sphere (nanoparticle/crystallite) with the substrate. This total adhesion force is plotted against the small particle radius in Figure 8c. This simulation indicated that the total vdW adhesion force should exhibit a minimum value as a function of the nanosphere radius, which was in qualitative agreement with the data in Figure 6. It was assumed in this model that only one echini tip of the replica contacted the metal substrate. This assumption was found to be reasonable in a previous study of magnetite pollen replica adhesion.[6f] The contacting nanoparticles/crystallites were also assumed to be uniform spheres. The range of measured radii of nanoparticles on the spine tips varied by less than 30% (Figure 4). Nonetheless, quantitative agreement of this model with the experimental data was not expected in light of other simplifying assumptions. For example, in summing the individual adhesion of each nanoparticle with the flat substrate, the interactions of any permanent or induced dipoles in the crystals or on the surface with one another were ignored. The individual nanoparticles were also assumed to be tightly packed on the spine tip surface. Despite these simple assumptions, the model did reveal a non-monotonic relationship between nanoparticle/crystal size and adhesion due to the counteracting effects of

Accepted Manuscript

nanoparticle/crystal size, and the number of nanoparticles/crystals in the vdW interaction zone, on the vdW adhesion force.

The conversion of sunflower pollen particles into replicas comprised of the spinel ferrite, $CoFe_2O_4$, endowed the replicas with a magnetic component to the adhesion force. AFM measurements were conducted to evaluate the adhesion force between individual $CoFe_2O_4$ replica particles (fired at different peak temperatures) and a Ni foil-coated, Nd-Fe-B alloy (axially-poled) permanent magnet (referred to simply as the Ni-Nd substrate). These force measurements were conducted at a lateral distance ~300 µm from the outer edge of the disk-shaped Ni-Nd substrate and measured at height intervals of 50 µm from the surface. The measured attraction forces for the $CoFe_2O_4$ replicas fired at peak temperatures of 600°C, 700°C, 800°C, and 900°C are shown in Figure 9a. This figure reveals a monotonic increase in the measured magnetic force of attraction with an increase in the peak firing temperature. Since these pollen replicas were coated in a similar fashion (i.e., with the same number of Co-O and Fe-O layers) and since these replicas were all comprised of phase-pure $CoFe_2O_4$ (Figure 3a), the observed increase in the magnetic force of attraction with peak firing temperature was attributed to the associated increase in average crystal size. Indeed, nanocrystalline $CoFe_2O_4$ has been previously reported to exhibit an increase in saturation magnetization and remanent magnetization with an increase in average crystal size (in the range of

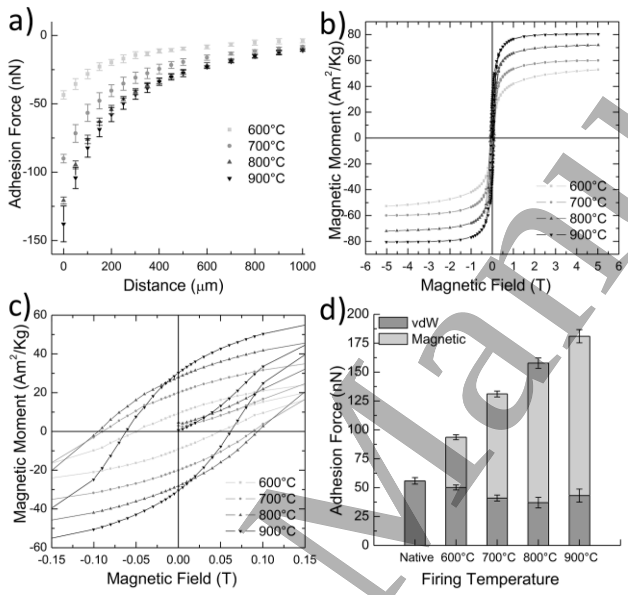

Figure 9. a) AFM measurements of the magnetic adhesion force experienced by $CoFe_2O_4$ sunflower replica probes vs. vertical distance from a Ni-Nd substrate. The force measurements were obtained at a lateral position ~300 µm from the edge of the disk-shaped Ni-Nd substrate. b), c) Superconducting Quantum Interference Device (SQUID) analyses of the magnetic moments of $CoFe_2O_4$ sunflower replicas (synthesized at various peak temperatures) vs. applied magnetic field at 300 K (a magnified view of the plot in b) is shown in c)). d) Combined short range (vdW) and short-to-long range (magnetic) adhesion for native sunflower pollen and $CoFe_2O_4$ sunflower pollen replicas.

< 10 nm to 100 nm).[20] To determine how the ferrimagnetic behavior of the $CoFe_2O_4$ pollen replicas changed with peak firing temperature and average crystal size, a SQUID magnetometer was used to evaluate the magnetic hysteresis of the pollen replicas at 5 K and at 300 K (via active temperature control). Distinct magnetic hysteresis loops, consistent with ferrimagnetic materials, were obtained for all samples (Figures 9b and 9c). As revealed by the data in Figures 9b and 9c and in Table 1, the values of saturation magnetization (M_s) and remanent magnetization (M_r) of the $CoFe_2O_4$ pollen replicas at both 5 K and 300 K increased with an increase in the peak

Table 1. Values of saturation magnetization (M_s) and remanent magnetization (M_r) of $CoFe_2O_4$ pollen replicas fired at different peak temperatures

Peak Temperature (°C)	M_s(5 K) (Am²/Kg)	M_r(5 K) (Am²/Kg)	M_s(300 K) (Am²/Kg)	M_r(300 K) (Am²/Kg)
600°C	58	38	53	9
700°C	67	46	60	20
800°C	78	52	72	27
900°C	85	54	80	30

firing temperature from 600°C to 900°C (and with an associated increase in average crystal radius from 5±2 nm to 38±6 nm).

Accepted Manuscript

Hence, by controlling the average crystal/nanoparticle size of the $CoFe_2O_4$ pollen replicas via adjustment of the peak firing temperature, the pollen magnetization and associated magnetic adhesion force (as well as the vdW adhesion force) could be tailored. The extent to which the total force of attraction (vdW and magnetic) of the $CoFe_2O_4$ pollen replicas could be tailored relative to native (cleaned) sunflower pollen is shown in a bar graph of the total adhesion force of such particles to the magnetic substrate in Figure 9d. The total force of adhesion of the $CoFe_2O_4$ replicas to the Ni-Nd substrate was greater by a factor of up to ~3 (for a peak firing temperature of 900°C) relative to the native pollen grains.

The present work demonstrates the ability to convert low-cost, sustainably-available, complex-shaped pollen templates into 3-D replica microparticles comprised of a multicomponent magnetic oxide compound with a tunable nanostructure for tailored adhesion. Such shape-preserving chemical conversion was accomplished via a scalable wet chemical SSG coating and firing process. Given the wide range of commercially-available metal alkoxides, this LbL SSG process may be used to convert pollen particles into numerous other multicomponent inorganic compounds with tailorable electromagnetic and other functional properties for controlled multimodal adhesion.

Conclusions

This work provides the first demonstration of: i) the conversion of pollen particles into high-fidelity 3-D replicas comprised of a multicomponent magnetic spinel ferrite (the compound $CoFe_2O_4$), and ii) the tailorability of short-range (van der Waals, vdW) and long-range (magnetic) adhesion forces acting on these 3-D bio-derived replicas through control of the sizes of the crystals/nanoparticles comprising these replicas.

A layer-by-layer, surface sol-gel (SSG) coating process was used to sequentially deposit Co-O-bearing and Fe-O-bearing layers (with an appropriate 1:2 cycle ratio) in a highly conformal manner onto sunflower pollen particle surfaces. Subsequent thermal treatment in air resulted in organic pyrolysis (removal of the underlying pollen template) and conversion of the coating into nanocrystalline, phase-pure $CoFe_2O_4$. The resulting $CoFe_2O_4$ particles retained the 3-D shapes and distinct surface features (notably the sharp spines/echini) of the starting sunflower pollen grains, as verified by examination of the same pollen grains before and after thermal treatment.

The short range (~10 nm) vdW force of adhesion between the $CoFe_2O_4$ pollen particle replicas and flat metallic (Au, Cu, Ni) substrates could be altered by adjusting the peak temperature used during thermal treatment of the pollen replicas. An increase in peak firing temperature from 600°C to 800°C resulted in a decrease in the vdW adhesion force, whereas a further rise in firing temperature from 800°C to 900°C resulted in an increase in this short-range force. This non-monotonic behavior was consistent with the counteracting effects of particle coarsening (observed by FEG-SEM analyses) on the size of nanoparticles, and the number of nanoparticles, present on the tips of the echini/spines and within the vdW interaction zone between the $CoFe_2O_4$ pollen replicas and the adjacent flat surfaces.

The long range (up to ~1 mm) magnetic force of adhesion between the pollen replicas and a flat magnetic (Ni-coated Nd-Fe-B permanent magnet) substrate could also be adjusted by controlling the peak firing temperature and the resulting average $CoFe_2O_4$ crystal size. An increase in the peak firing temperature from 600°C to 900°C resulted in an increase in the average $CoFe_2O_4$ crystal radius (as determined from full profile fitting of XRD patterns and Williamson-Hall analyses) from 5 ± 2 nm to 38 ± 6 nm. As previously reported for nanocrystalline $CoFe_2O_4$, this increase in crystal size coincided with increases in the values of the saturation and remanent magnetization of the $CoFe_2O_4$ pollen particle replicas (as determined from SQUID measurements) and a corresponding increase in the long-range adhesion of these replicas to a magnetic substrate.

The conversion of sunflower pollen particles into high-fidelity $CoFe_2O_4$ replicas that retained the 3-D shapes and surface features (sharp echini) of the starting pollen particles allowed for comparison of the adhesion of these replicas to the similarly-shaped native pollen particles. By adjusting the $CoFe_2O_4$ crystal/nanoparticle sizes of the replicas, the total force of adhesion to a magnetic substrate could be increased by a factor of up to ~3 relative to the native pollen grains.

Acknowledgements

The research was supported by the U.S. Air Force Office of Scientific Research via Award No. FA9550-10-1-0555. The research work of S.H., and the manuscript preparation and editing work of K.H.S., were supported by the U.S. Department of Energy via Award No. DE-SC0014034.

Accepted Manuscript

Notes and references

The authors declare no competing financial interest.

Abbreviations AFM, atomic force microscopy; DIW, de-ionized water; EDS, energy-dispersive X-ray spectroscopy; FEG SEM, field emission gun scanning electron microscope; FIB, focused ion beam milling; ICP-MS, inductively coupled plasma – mass spectroscopy; IPA, isopropyl alcohol; LbL, layer-by-layer; Ni, polished nickel foil; Ni-Nd, polished nickel foil-coated, neodymium-iron-boron alloy permanent magnet disk; NIST, National Institute of Standards and Technology; RC, average crystallite radius; RMS, root mean square; SE, secondary electron; SPM, scanning probe microscope; SQUID, superconducting quantum interference device; SSG, surface sol-gel; TEM, transmission electron microscopy; TG, thermogravimetric; 3-D, three-dimensional; vdW, van der Waals; XRD, X-ray diffraction

1 (a) Ott, M. L.; Mizes, H. A. Atomic Force Microscopy Adhesion Measurements of Surface-Modified Toners for Xerographic Applications. *Colloids Surfaces A: Physicochem. Eng. Aspects* **1994,** *87* (3), 245-256; (b) Wen, W.; Wang, N.; Zheng, D. W.; Chen, C.; Tu, K. N. Two- and Three-Dimensional Arrays of Magnetic Microspheres. *J. Mater. Res.* **1999,** *14 (4)*, 1186-1189; (c) Bowen, W.R.; Doneva, T. A. Atomic Force Microscopy Studies of Membranes. Effect of Surface Roughness on Double-Layer Interactions and Particle Adhesion. *J. Colloid Interface Sci.* **2000,** *229* (2), 544-549; (d) Meitl, M. A.; Zhu, Z. T.; Kumar, V.; Lee, K. J.; Feng, X.; Huang, Y. Y.; Adesida, I.; Nuzzo, R. G.; Rogers, J. A. Transfer Printing by Kinetic Control of Adhesion to an Elastomeric Stamp. *Nat. Mater.* **2006,** *5 (1)*, 33-38; (e) Spettmann, D.; Eppmann, S.; Flemming, H.-C.; Wingender, J. Simultaneous Visualization of Biofouling, Organic and Inorganic Particle Fouling on Separation Membranes. *Water Sci. Technol.* **2007**, *55* (8-9) 207-210; (f) Mitragotri, S.; Lahann, J. Physical Approaches to Biomaterial Design. *Nat. Mater.* **2009,** *8 (1)*, 15-23; (g) Huang, Y.; Liu, M.; Wang, J.; Zhou, J.; Wang, L.; Song, Y.; Jiang, L. Controllable Underwater Oil-Adhesion-Interface Films Assembled from Nonspherical Particles. *Adv. Funct. Mater.* **2011,** *21* (23), 4436-4441; (h) Fischer, K. E.; Nagaraj, G.; Daniels, R. H.; Li, E.; Cowles, V. E.; Miller, J. L.; Bunger, M. D.; Desai, T. A. Hierarchical Nanoengineered Surfaces for Enhanced Cytoadhesion and Drug Delivery. *Biomater.* **2011,** *32 (13)*, 3499-3506; (i) Stassi, S.; Canavese, G. Spiky Nanostructured Metal Particles as Filler of Polymeric Composites Showing Tunable Electrical Conductivity. *J. Polym. Sci., Part B* **2012,** *50 (14)*, 984-992; (j) Indalkar, Y.R.; Gaikwad, S.S.; Ubale, A.T. Janus Particles Recent and Novel Approach in Drug Delivery: An Overview. *Current Pharma Res.* **2013**, *3* (4) 1031-1037; (k) Xiao, G.; Su, H.; Tan, T. Synthesis of Core-Shell Bioaffinity Chitosan-TiO2 Composite and Its Environmental Applications. *J. Hazard. Mater.* **2015**, *283*, 888-896.

2 (a) Rosi, N. L.; Thaxton, C. S.; Mirkin, C. A. Control of Nanoparticle Assembly by Using DNA-Modified Diatom Templates. *Angew. Chem., Int. Ed.* **2004,** *43* (41), 5500-5503; (b) Gaddis, C. S.; Sandhage, K. H. Freestanding Microscale 3D Polymeric Structures with Biologically-derived Shapes and Nanoscale Features. *J. Mater. Res.* **2004,** *19 (9)*, 2541-2545; (c) Payne, E. K.; Rosi, N. L.; Xue, C.; Mirkin, C. A. Sacrificial Biological Templates for the Formation of Nanostructured Metallic Microshells. *Angew. Chem., Int. Ed.* **2005,** *44* (32), 5064-5067; (d) Zhao, J.P.; Gaddis, C. S.; Cai, Y.; Sandhage, K. H. Freestanding Microscale Structures of Nanocrystalline Zirconia with Biologically Replicable Three Dimensional Shapes. *J. Mater. Res.* **2005,** *20 (2)*, 282-287; (e) Weatherspoon, M.R.; Allan, S.M.; Hunt, E.; Cai, Y.; Sandhage, K.H. Sol-Gel Synthesis on Self-Replicating Single-Cell Scaffolds: Applying Complex Chemistries to Nature's 3-D Nanostructured Templates. *Chem. Comm.* **2005**, (5) 651-653; (f) Weatherspoon, M. R.; Haluska, M. S.; Cai, Y.; King, J. S.; Summers, C. J.; Snyder, R. L.; Sandhage, K. H. Phosphor Microparticles of Controlled Three-Dimensional Shape from Phytoplankton. *J. Electrochem. Soc.* **2006,** *153*, H34-H37; (g) Losic, D.; Mitchell, J. G.; Lai, R.; Voelcker, N. H. Rapid Fabrication of Micro- and Nanoscale Patterns by Replica Molding from Diatom Biosilica. *Adv. Funct. Mater.* **2007,** *17*, 2439-2446; (h) Kusari, U.; Bao, Z.; Cai, Y.; Ahmad, G.; Sandhage, K. H.; Sneddon, L. G. Formation of Nanostructured Boron Nitride Microparticles with Diatom-Derived 3-D Shapes. *Chem. Commun.* **2007,** *11*, 1177-1179; (i) Bao, Z.; Ernst, E. M.; Yoo, S.; Sandhage, K. H. Syntheses of Porous Self-Supporting Metal Nanoparticle Assemblies with 3-D Morphologies Inherited from Biosilica Templates (Diatom Frustules). *Adv. Mater.* **2009,** *21* (4), 474-478; (j) Fang, Y.; Berrigan, J.D.; Cai, Y.; Marder, S.R.; Sandhage, K.H. Syntheses of Nanostructured Cu- and Ni-based Micro-assemblies with Selectable 3-D Hierarchical Biogenic Morphologies. *J. Mater. Chem.* 2012, *22* (4), 1305-1312; (k) Fang, Y.; Chen, V.W.; Cai, Y.; Berrigan, J.D.; Marder, S.R.; Perry, J.W.; Sandhage, K.H. Biologically-Enabled Syntheses of Freestanding Metallic Structures Possessing Subwavelength Pore Arrays for Extraordinary (Plasmon-Mediated) Infrared Transmission. *Adv. Funct. Mater.* **2012**, *22* (12) 2550-2559.

3 (a) Anderson, M. W.; Holmes, S. M.; Hanif, N.; Cundy, C. S. Hierarchical Pore Structures Through Diatom Zeolitization. *Angew. Chem., Int. Ed.* **2000,** *39* (15), 2707-2710; (b) Sandhage, K.H.; Dickerson, M.B.; Huseman, P.M.; Caranna, M.A.; Clifton, J.D.; Bull, T. A. Bull; Heibel, T.J.; Overton, W.R.; Schoenwaelder, M.E.A. Novel, Bioclastic Route to Self-Assembled, 3D, Chemically Tailored Meso/Nanostructures: Shape-Preserving Reactive Conversion of Biosilica (Diatom) Microshells. *Adv. Mater.* **2002**, *14* (6) 429-433; (c) Unocic, R.R.; Zalar, F.M.; Sarosi, P.M.; Cai, Y.; Sandhage, K.H. Anatase Assemblies from Algae: Coupling Biological Self-assembly of 3-D Nanoparticle Structures with Synthetic Reaction Chemistry," *Chem. Comm.* **2004**, (7) 795-796; (d) Sandhage, K.H.; Snyder, R.L.; Ahmad, G.; Allan, S.M.; Cai, Y.; Dickerson, M.B.; Gaddis, C.S.; Haluska, M.S.; Shian, S.; Weatherspoon, M.R.; Rapp, R.A.; Unocic, R.R.; Zalar, F.M.; Zhang, Y.; Hildebrand, M.; Palenik, B.P. Merging Biological Self-Assembly with Synthetic Chemical Tailoring: The Potential for 3-D Genetically-Engineered Micro/Nanodevices (3-D GEMS). *Int. J. Appl. Ceram. Technol.* **2005**, *2* (4) 317-326; (e) Cai, Y.; Allan, S.M.; Zalar, F.M., Sandhage, K.H. Three-Dimensional Magnesia-Based Nanocrystal Assemblies via Low-Temperature Magnesiothermic Reaction of Diatom Microshells. *J. Am. Ceram. Soc.* **2005**, *88* (7), 2005-2010; (f) Shian, S.; Cai, Y.; Weatherspoon, M.R.; Allan,

Accepted Manuscript

S.M.; Sandhage, K.H. Three-Dimensional Assemblies of Zirconia Nanocrystals via Shape-Preserving Reactive Conversion of Diatom Microshells. *J. Am. Ceram. Soc.* **2006**, *89* (2), 694-698; (g) Lee, S.-J.; Shian, S.; Huang, Ch.-H.; Sandhage, K.H. Rapid, Non-Photocatalytic Destruction of Organophosphorous Esters Induced by Nanostructured Titania-Based Replicas of Diatom Microshells. *J. Am. Ceram. Soc.* **2007**, *90* (5), 1632-1636; (h) Bao, Z.; Weatherspoon, M.R.; Cai, Y.; Shian, S.; Graham, P.D.; Allan, S.M.; Ahmad, G.; Dickerson, M.B.; Church, B.C.; Kang, Z.; Summers, C.J.; Abernathy, H.W.; Liu, M.; Sandhage, K.H. Shape-Preserving Reduction of Silica Micro-Assemblies into Microporous Silicon Replicas. *Nature* **2007**, *446* (3), 172-175; (i) Sandhage, K.H. Materials 'Alchemy': Shape-preserving Chemical Transformation of Micro-to-Macroscopic 3-D Structures. *JOM* **2010**, *62* (6), 32-43; (j) Davis, S.C.; Sheppard, V.C.; Begum, G.; Cai, Y.; Fang, Y.; Berrigan, J.D.; Kröger, N.; Sandhage, K.H. Rapid Flow-through Biocatalysis with High Surface Area, Enzyme-loaded Carbon and Gold-bearing Diatom Frustule Replicas. *Adv. Funct. Mater.* **2013**, *23* (36) 4611-4620; (k) Xia, Z.; Davis, S.C.; Eftekhar, A.A.; Gordin, A.S.; Askari, M.; Li, Q.; Ghasemi, F.; Sandhage, K.H.; Adibi, A, Magnesiothermically-Formed Porous Silicon Thin Films on Silicon-on-Insulator Optical Microresonators for High-Sensitivity Detection. *Adv. Optical Mater.* **2014**, ***2*** (3) 235-239.

4 (a) Kremp, G. O. W. *Morphologic Encyclopedia of Palynology,* 2nd ed.; University of Arizona Press: Tucson, AZ, USA, 1968. (b) Erdtman, G. *Pollen Morphology and Plant Taxonomy*; E. J. Brill: Leiden, The Netherlands, 1986. (c) Blackmore, S.; Barnes, S. H. (eds.) *Pollen and Spores: Patterns of Diversification*; Clarendon Press: Oxford, UK, 1991. (d) Beggs, P. J. Impacts of Climate Change on Aeroallergens: Past and Future. *Clin. Exp. Allergy* **2004**, *34* (10), 1507-1513; (e) Tanaka, N.; Uehara, K.; Murata, J. Correlation Between Pollen Morphology and Pollination Mechanisms in the Hydrocharitaceae. *J. Plant Res.* **2004,** *117* (4), 265-276. (f) Hesse, M.; Halbritter, H.; Zetter, R.; Weber, M.; Buchner, R.; Frosch-Radivo, A.; Ulrich, S. *Pollen Terminology: An Illustrated Handbook*; Springer-Verlag: New York, NY, USA, 2009; (g) Ziska, L.; Knowlton, K.; Rogers, C.; Dalan, D.; Tierney, N.; Elder, M. A.; Filley, W.; Shropshire, J.; Ford, L. B.; Hedberg, C.; Fleetwood, P.; Hovanky, K. T.; Kavanaugh, T.; Fulford, G.; Vrtis, R. F.; Patz, J. A.; Portnoy, J.; Coates, F.; Bielory, L.; Frenz, D. Recent Warming by Latitude Associated with Increased Length of Ragweed Pollen Season in Central North America. *Proc. Nat. Acad. Sci. U.S.A.* **2011**, *108* (10), 4248-4251. (h) Lin, H.; Gomez, I.; Meredith, J.C. Pollenkitt Wetting Mechanism Enables Species-Specific Tunable Pollen Adhesion. *Langmuir* **2013,** *29* (9), 3012-3023.

5 (a) Hall, S. R.; Bolger, H.; Mann, S. Morphosynthesis of Complex Inorganic Forms Using Pollen Grain Templates. *ChemComm* **2003,** (22), 2784-2785; (b) Wang, Y.; Liu, Z.; Han, B.; Sun, Z.; Du, J.; Zhang, J.; Jiang, T.; Wu, W.; Miao, Z. Replication of Biological Organizations Through a Supercritical Fluid route. *ChemComm* **2005,** (23), 2948-2950; (c) Hall, S. R.; Swinerd, V. M.; Newby, F. N.; Collins, A. M.; Mann, S. Fabrication of Porous Titania (Brookite) Microparticles with Complex Morphology by Sol-Gel Replication of Pollen Grains. *Chem. Mater.* **2006,** *18*, 598-600; (d) Cao, F.; Li, D. X. Morphology-Controlled Synthesis of SiO_2 Hollow Microspheres Using Pollen Grain as a Biotemplate. *Biomedical materials* **2009,** *4* (2), 1-6; (e) Yang, X.; Song, X.; Wei, Y.; Wei, W.; Hou, L.; Fan, X. Synthesis of Spinous ZrO_2 Core–Shell Microspheres with Good Hydrogen Storage Properties by the Pollen Bio-Template Route. *Scr. Mater.* **2011,** *64* (12), 1075-1078; (f) Thio, B. J.; Clark, K. K.; Keller, A. A. Magnetic Pollen Grains as Sorbents for Facile Removal of Organic Pollutants in Aqueous Media. *J. Hazard. Mater.* **2011,** *194*, 53-61; (g) Xia, Y.; Zhang, W.; Xiao, Z.; Huang, H.; Zeng, H.; Chen, X.; Chen, F.; Gan, Y.; Tao, X., BioTemplated Fabrication of Hierarchically Porous NiO/C Composite from Lotus Pollen Grains for Lithium-Ion Batteries. *J. Mater. Chem.* **2012,** *22* (18), 9209-9215.

6 (a) Ichinose, I.; Senzu, H.; Kunitake, T. Stepwise Adsorption of Metal Alkoxides on Hydrolyzed Surfaces: A Surface Sol-Gel Process. *Chem. Lett.* **1996,** *10*, 831-832; (b) Ichinose, I.; Senzu, H.; Kunitake, T., A Surface Sol-Gel Process of TiO_2 and Other Metal Oxide Films with Molecular Precision. *Chem. Mater.* **1997,** *9*, 1296-1298; (c) Weatherspoon, M.R.; Cai, Y.; Crne, M.; Srinivasarao, M.; Sandhage, K.H. 3-D Rutile Titania-based Structures with *Morpho* Butterfly Wing Scale Morphologies. *Angew. Chem. Int. Ed.* **2008**, *47* (41), 7921-7923; (d) Vernon, J.P.; Fang, Y.; Cai, Y.; Sandhage, K.H. Morphology-preserving Conversion of a 3D Bio-organic Template into a Nanocrystalline Multicomponent Oxide Compound. *Angew. Chem. Intl. Ed.* **2010**, *49*, 7765-7768; (e) Vernon, J.P.; Hobbs, N.; Lethbridge, A.; Vukusic, P.; Deheyn, D.D.; Sandhage, K.H. 3-D Photoluminescent Lanthanide-doped Barium Titanate Structures Synthesized by Coating and Shape-preserving Reaction of Complex-shaped Bioorganic Templates. *J. Mater. Chem.* **2012**, ***22*** (21), 10435-10437; (f) Goodwin, W.B.; Gomez, I. J.; Fang, Y.; Meredith, J. C.; Sandhage, K. H. Conversion of Pollen Particles into Three-Dimensional Ceramic Replicas Tailored for Multimodal Adhesion. *Chem. Mater.* **2013,** *25* (22), 4529-4536; (g) Gomez, I.J.; Goodwin, W.B.; Sabo, D.; Zhang, Z.J.; Sandhage, K.H.; Meredith, J.C. Three-Dimensional Magnetite Replicas of Pollen Particles with Tailorable and Predictable Multimodal Adhesion. *J. Mater. Chem. C* **2015**, *3* (3), 632-643.

7 Dobson, H. E. M. Survey of Pollen and Pollenkitt Liquids - Chemical Cues to Flower Visitors? *Am. J. Botany* **1988**, *75* (2), 170-182.

8 (a) Weatherspoon, M.R.; Dickerson, M.B.; Wang, G.; Cai, Y.; Shian, S.; Jones, S.C.; Marder, S.R.; Sandhage, K.H. Thin, Conformal, and Continuous SnO_2 Coatings on Hydroxyl-Amplified Biosilica (Diatom) Templates via Layer-by-Layer Alkoxide Deposition. *Angew. Chem. Int. Ed.* **2007**, *46*, 5724-5727; (b) Fang, Y.; Wu, Q.; Dickerson, M. B.; Cai, Y.; Shian, S.; Berrigan, J. D.; Poulsen, N.; Kröger, N.; Sandhage, K. H., Protein-Mediated Layer-by-Layer Syntheses of Freestanding Microscale Titania Structures with Biologically Assembled 3-D Morphologies. *Chem. Mater.* **2009,** *21* (24), 5704-5710; (c) Wang, G.; Fang, Y.; Kim, P.; Hayek, A.; Weatherspoon, M.R.; Perry, J.W.; Sandhage, K.H.; Marder, S.R.; Jones, S.C. Layer-by-Layer Dendritic Growth of Hyperbranched Thin Films for Surface Sol-Gel Syntheses of Conformal, Functional, Nanocrystalline Oxide Coatings on Complex 3-D (Bio)Silica Templates. *Adv. Funct. Mater.* **2009**, *19* (17) 2768-2776.

9 Fransen, M. J. On The Influence of Generators and Detector Settings in X-ray Powder Diffractometry. *Adv. X-ray Anal.* **2005,** *48*, 143-149.

10 Cullity, B.D.; Stock, S.R. *Elements of X-Ray Diffraction*, 3rd ed.; Prentice-Hall, Inc., Upper Saddle River, NJ, USA, 2001.

Accepted Manuscript

11 Domínguez, E.; Mercado, J. A.; Quesada, M. A.; Heredia, A. Pollen Sporopollenin: Degradation and Structural Elucidation. *Sex. Plant Reprod.* **1999**, *12* (3), 171-178.

12 Takahashi, M.; Fine, M.E. Coercive Force of Spinodally Decomposed Cobalt Ferrite with Excess Cobalt. *J. Am. Ceram. Soc.* **1970**, 53 (11), 633-634.

13 Card No. 96-591-0064 for $CoFe_2O_4$; International Center for Diffraction Data: Newtown Square, PA USA, 2007.

14 Caglioti, G.; Paoletti, A.; Ricci, F.P. Choice of Collimaors for a Crystal Spectrometer for Neutron Diffraction. *Nucl. Inst.* **1958**, *3*, 223-228.

15 Williamson, G.K.; Hall, W.H. X-ray Line Broadening from Filed Aluminum and Tungsten. Acta Metall. 1953, 1 (1), 22-31.

16 (Hamaker, H. C. The London-van der Waals Attraction Between Spherical Particles. Physica 1937, 4, 1058-1072.

17 Israelachvili, J., Intermolecular and Surface Forces, 2nd ed., Academic Press: London, UK, 1992.

18 Fernández, M.B.; Zélis, P.M.; Coral, D.F.; Torres, T.E.; Marquina, C.; Goya, G.F.; Sánchez, F.H. Self Organization in Oleic Acid-Coated $CoFe_2O_4$ Colloids: A SAXS Study. J. Nanopart. Res. 2012, 14, 1072-1082.

19 Thio, B. J. R.; Lee, J.-H.; Meredith, J. C. Characterization of Ragweed Pollen Adhesion to Polyamides and Polystyrene Using Atomic Force Microscopy. Environ. Sci. Technol. 2009, 43 (12), 4308-4313.

20 (a) Rajendran, M.; Pullar, R.C.; Bhattacharya, A.K.; Das, D.; Chintalapudi, S.N.; Majundar, C.K. Magnetic Properties of Nanocrystalline $CoFe_2O_4$ Powders Prepared at Room Temperature: Variation with Crystallite Size. J. Magn. Magn. Mater. 2001, 232, 71-83; (b) Kumar, V.; Rana, A.; Yadav, M. S.; Pant, R. P. Size-Induced Effect on Nano-Crystalline $CoFe_2O_4$. J. Magn. Magn. Mater. 2008, 320 (11), 1729-1734.

Accepted Manuscript